How does Silica Catalyze the Amide Bond Formation in Dry Conditions? Role of Specific Surface Silanol Pairs

How does Silica Catalyze the Amide Bond Formation in Dry Conditions? Role of Specific Surface Silanol Pairs

Albert Rimola,[*†] *Marco Fabbiani,*[*‡] *Mariona Sodupe,*[†] *Piero Ugliengo*[*§] *and Gianmario Martra*[§]

† *Departament de Química, Universitat Autònoma de Barcelona, 08193 Bellaterra, Spain.*

‡ *Dipartimento di Scienza e Alta Tecnologia, Università degli Studi dell'Insubria, Via Valleggio 11, 22100 Como, Italy.*

§ *Dipartimento di Chimica and Nanostructured Interfaces and Surfaces (NIS) Inter-Departmental centre, Università degli Studi di Torino, Via P. Giuria 7, 10125 Torino, Italy.*

CORRESPONDING AUTHORS

The manuscript was written through contributions of all authors. All authors have given approval to the final version of the manuscript. (*) These authors contributed equally.

* albert.rimola@uab.cat

* mfabbiani@uninsubria.it

* piero.ugliengo@unito.it

ABSTRACT

The mechanism of the amide bond formation between non-activated carboxylic acids and amines catalyzed by the surface of amorphous silica in dry conditions is elucidated by combining spectroscopic measurements and quantum chemical simulations. Results suggest a plausible explanation of the catalytic role of silica in the reaction. Both experiment and theory identify very weakly interacting SiOH surface group pairs (*ca*. 5 Å apart) as key specific sites for simultaneously hosting, in the proper orientation, ionic and canonical pairs of the reactants. An atomistic interpretation of the experiments indicates that this coexistence is crucial for the occurrence of the reaction, since the components of canonical pair are those undergoing the amidation reaction while the ionic pair directly participates in the final dehydration step. Transition state theory based on quantum mechanical free energy potential energy shows the silica-catalyzed amide formation as relatively fast. The work also points out that the presence of the specific SiOH group pairs is not exclusive of the adopted silica sample, as they can also be present in natural forms of silica, for instance as hydroxylation defects on α-quartz, so that they could exhibit similar catalytic activity towards the amide bond formation.

KEYWORDS

direct amidation reaction mechanism, heterogeneous catalysis, surface chemistry, prebiotic chemistry, IR spectroscopy, cluster and periodic DFT simulations

INTRODUCTION

Formation of amides by condensation of amines and carboxylic acids is a subject of paramount interest from both industrial and fundamental perspectives.[1] In industry, the amide bond (AB) formation is a key reaction for pharmaceutical companies, by the adoption of powerful activating agents in the current synthetic routes. Unfortunately, they are both expensive, because of a poor atom economy, and environmentally unfriendly. [1] Thus, developing clean and low cost synthetic strategies with good atom economy is highly pursued.[2] Homogeneous catalytic routes have been developed,[3-7] as well as synthetic methods based on heterogeneous catalysts. Active materials are noble metals nanoparticles,[8] but also common oxides such as SiO_2, TiO_2, ZnO were found to exhibit promising performances towards the catalyzed AB formation.[9-12] Noteworthy, the exploitation of these catalytic materials contributes to the continuous search for heterogeneous catalysts non-based on noble/rare metals. The design of highly efficient oxide catalyst for AB formation also requires the elucidation of reaction mechanisms occurring at their surface. Relevant insights on a mechanistic elucidation have recently been reported for homogeneous catalyzed direct amidation.[13] Conversely, to the best of our knowledge, there is no equivalent for direct amidation on surface oxides. Moreover, understanding the AB formation is also of fundamental importance, as it regulates the condensation of amino acids for the peptide synthesis, with profound implications in prebiotic chemistry and origin of life theories. Among the sequence of the organization events leading to the emergence of life, the peptide bond formation is still a not-well understood step, which is critical in the formation of the first biopolymers. From the seminal work of the British biophysicist Bernal,[14] to more recent proposals by Smith[15] and Orgel,[16] a wide consensus on the key role of mineral surfaces in

favoring this reaction has been reached, as they present proper surface sites that can adsorb and concentrate amino acids, as well as lower the activation barrier.

Based on these proposals, intensive investigations of the catalytic amide/peptide bond formation on mineral surfaces from experimental (*e.g.*,[17-22]) and computational (*e.g.*,[23-25]) viewpoints have been done and reviewed.[26-30] Obviously, rationalization of these results would provide relevant hints on the role of mineral surfaces in the AB formation, but this can also be a daunting task since, just for the limited case of silica surfaces, they present a sheer variety of structures and pre-reaction treatments.

A milestone common to both synthetic and prebiotic chemistry is the obvious "water problem" (*i.e.*, in water solution the reaction is disfavored). Nevertheless, the elucidation of how it could have been overcome on the prebiotic Earth is not straightforward. An interesting hypothesis is based on daily fluctuations of temperature and seasonal fluctuations of humidity, which readily occurs under natural conditions. They could have led to cycles of drying and rewetting so that condensation reactions become possible during the drying cycle of a wetting/drying cycle. This theory is supported by experimental evidences, provided by. Lahav et al.[17] and Muller and Schulze-Makuch.[31]

The aim of the present work is to provide a deep understanding of the AB formation mechanism on silica surfaces and determining the actual role of the surfaces in the process, focusing on molecular phenomena occurring during the dry conditions. This has been done by combining synergistically IR spectroscopy measurements with quantum chemical calculations. To make the study more tractable, present work is constrained on the experiments by Martra et al.,[19] where polyglycines were produced admitting glycine vapor on silica. Here, to avoid the progressive

polymerization of glycine and to focus only on the specific AB condensation reaction, in the experiments, glycine is replaced by formic acid and 1-pentanamine or methylamine. Pure silica (SiO_2) is a solid compound consisting of a network of [SiO_4] tetrahedral units that are connected in different ways giving rise to the different silica polymorphs, including crystalline and amorphous/glassy materials. At room temperature and low pressure, the most stable silica phase is α-quartz, followed by α-tridymite and α-cristobalite, which are also the most common high-density crystalline polymorphs. Bare silica surfaces are characterized to present siloxane (Si-O-Si) and silanol (Si-OH) groups. These chemical functionalities impart the hydrophobic/hydrophilic character to the silica surface. The nature, density and distribution of these surface functionalities determine the physico-chemical properties of silica surfaces, and in particular the adsorptive features. In the present work, AEROSIL®OX50, a highly pure pyrogenic amorphous SiO_2 powder, was used. Noteworthy, silicas of the AEROSIL® type were used in several studies on the abiotic polymerization of amino acids,[19, 22, 27] and, very recently, on the formation of a nucleoside (adenosine monophosphate) and one of its molecular precursor under prebiotic conditions.[32] AEROSIL®OX50 was selected for the purpose of this work because of its specific surface area (SSA) of *ca*. 50 m^2/g. This SSA is, on one side, high enough to obtain clearly detectable IR signals of surface species, while on the other side, low enough to be unaffected by calcination up to 973 K *(vide infra*). Thus, the removal of surface silanols without changes of the texture of material is attained.

RESULTS AND DISCUSSION

Evolution of surface silanol population along step-wise thermal treatment

The amorphous silica surface, depending on the method of preparation, exhibits Si-OH groups which are usually in relatively strong mutual hydrogen bond (H-bond) interaction. When silica samples are heated at increasing temperature under continuous pumping, a dehydration process occurs involving the condensation of hydrogen bonded SiOH groups with the formation of siloxane bond (Si-O-Si) and water, usually removed during the pumping process. The dehydration process is complex and it is highly dependent on the nature of the considered silica; *i.e.*, it depends on the silanol distribution. During the dehydration progress, the silica surface will become less rich in SiOH groups, eventually ending up with just isolated Si-OH group. These groups are well far apart (about one Si-OH *per* nm^2) and are surrounded by Si-O-Si bonds. The hydrophobic character is also increased during the process (the Si-O-Si bond dominates over the Si-OH groups), driving the adsorption of molecules through dispersive interaction rather than through hydrogen bond with the Si-OH groups. During a high temperature treatment, it can also occur that pair of Si-OH groups will condense, giving rise to highly strained (and therefore reactive toward adsorbed molecules) $(Si\text{-}O)_2$ and $(Si\text{-}O)_3$ rings. A key point of the experimental part of the present work was the setup of proper thermal treatment conditions, which allows: i) a selective, progressive removal of distinct families of silanols (SiOH) differing in strength of mutual H-bond interactions because of the different inter-silanol distance, and ii) any presence of surface strained siloxane bridges (*vide supra*). The point ii) is crucial, as such bridges are known to be reactive with amine and carboxylic acids, as well as H_2O molecules,[33] all of them being species involved in our reaction of interest. These targets were successfully attained by calcination in static air at 723 K and then at 973 K (details on the heating rate and duration of

isothermal treatments are available in the Methods section). As anticipated above, the SSA remained unchanged, even after calcination at the highest temperature (see Table 1).

Table 1 Specific surface area (SSA_{BET}) of silica samples in the pristine form and after calcination in air at 723 and 973 K. The accuracy of the measurement is *ca* ± 5%.

Sample	SSA_{BET} ($m^2\ g^{-1}$)
Pristine	47 ± 3
Calcined in air at 723 K	47 ± 3
Calcined in air at 973 K	49 ± 3

For the sake of completeness, we also assessed the invariance of both XRD pattern and Raman spectrum (see Figure S1 of the Supporting Information, SI).

Through IR spectroscopy in a controlled atmosphere we monitored the effect of the thermal treatments on surface silanols. Evidence of the irreversibility of the removal of silanols towards subsequent contact with water is depicted in Figure 1. The ν(OH) spectrum of pristine, thermally untreated silica outgassed at beam temperature (hereafter b.t.) appears composed by (Figure 1A, curve a) a narrow peak at 3747 cm^{-1} due to "isolated" silanols (*i.e.*, not involved in any inter-silanol interaction), and by a complex and broad absorption, asymmetric over the low frequency side, due to interacting surface silanols and intraglobular Si-OH (*vide infra)*.[34] The pattern in the 2100-1500 range is due to combination (1995 and 1870 cm^{-1}) and overtone (1630 cm^{-1}) modes of the silica bulk network,[34] and was used to normalize the spectra of different samples with respect to the same silica amount. A H/D isotopic exchange was carried out by replicating D_2O vapor

(20 mbar) admission/outgassing steps until invariance of the spectra (Figure 1A, curve b). Typically, 5 cycles ensured a full exchange. Surface silanols, now in the Si-OD form, produced the ν(OD) pattern in the 2800-2100 cm^{-1} range, whereas the ν(OH) pattern in the 3750-3000 cm^{-1} range monitors the presence of intra-globular Si-OH, which are not accessible to H/D exchange.[34] Noteworthy, evidence of the complete desorption of water molecules from the silica surface by outgassing at b.t. is provided by absence of changes in the 1700-1600 cm^{-1}, where the δ(H_2O) signal, if present, should disappear in favor of the downshifted δ(D_2O) one. As expected, a D/H isotopic back exchange by contact with 20 mbar of H_2O vapor fully restored the initial spectrum of the pristine silica sample outgassed at b.t. (Figure 1A, curve c).

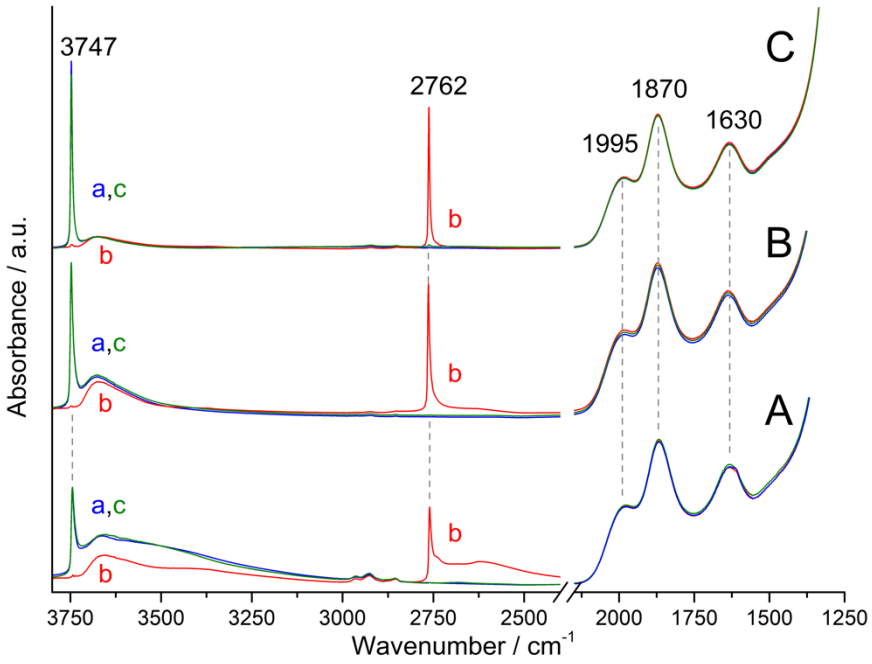

Figure 1. IR spectra of SiO_2 samples: A) in the pristine form; B) calcined at 723 K; C) calcined at 973 K. In each section: a) sample outgassed at b.t.; b) after isotopic H/D exchange by admission (20 mbar)/outgassing at b.t. of D_2O vapor; c) after isotopic D/H back exchange, by admission (20 mbar)/outgassing at b.t. of H_2O vapor.

Equivalent sets of spectra were acquired for silica samples calcined at 723 K (Figure 1B) and at 973 K (Figure 1C). In the following, we describe the effect of thermal treatments on surface silanols. It is worth mentioning that also for these cases the final contact with H_2O vapor and subsequent outgassing restored the spectra obtained after the initial outgassing at b.t (curves a and c in Fig 1B and 1C), thus witnessing for the absence of reactive surface strained siloxane bridges. Moreover, the H/D exchange reveals that thermal treatment also promoted the condensation between intra-globular silanols (curves b in Figure 1B and 1C).

For each sample, the subtraction of the ν(OH) pattern of intra-globular silanols (curves b) from that obtained after initial outgassing at b.t (curves a) allows to obtain the ν(OH) spectral profile due to surface Si-OH only. The results are shown in Figure 2A. For the pristine SiO_2 (curve a), the ν(OH) pattern of surface silanols is constituted by: i) the narrow peak at 3747 cm^{-1} due to isolated SiOH, asymmetric on the low frequency side, ii) a shoulder at 3720 cm^{-1} (SiOH terminating chains of interacting silanols), iii) an ill resolved sub-band at 3665 cm^{-1} (weakly H-bonded silanols), and iv) a broad component with maximum at 3530 cm^{-1} (asymmetric down to 3000 cm^{-1}) due to H-bonded SiOH.[34] ν(OH) signals below 3735 cm^{-1} were almost depleted by thermal treatment at 723 K (Figure 2A, curve b), monitoring the removal of the overwhelming part of H-bonded silanols. This depletion is accompanied by an increase in intensity of the peak at 3747 cm^{-1}, still asymmetric on the low frequency side, due to the additional contribution of silanols that remained isolated after removal of their interacting partner(s). By increasing the temperature treatment up to 973 K, condensation of all types of surface silanols absorbing below *ca.* 3730 cm^{-1} appeared completed, and the peak at 3747 cm^{-1} becomes narrower and more symmetric and intense (for the same reason indicated above). A clearer and more detailed view of the evolution of the surface silanols population, as monitored through the ν(OH) pattern, is

provided by the difference between the spectra of the silica before and after each step of the thermal treatment (Figure 2B). The correctness and effectiveness of this spectral subtraction is guaranteed by the possibility to normalize the original spectra with respect to the mass of silica and the constancy on the SSA. The difference between the spectra of the sample calcined at 723 K and the pristine one (Figure 2B, curve b-a) results in a broad negative band, with the high frequency onset at 3735 cm^{-1}, constituted by the overlapping of several components, located at lower frequency as the strength of inter-silanols interaction (likely of the H-bond type) increases. The difference between the spectra of samples calcined at 973 or at 723 K (Figure 2B, curve c-b) provides evidence that the increase of the calcination temperature mainly results in the removal of very weakly interacting silanols, characterized by a ν(OH) of 3742 cm^{-1} (minimum of the negative part of the difference spectrum). In both difference spectra, the sharp peak at 3747 cm^{-1} is due to the newly formed isolated silanols.

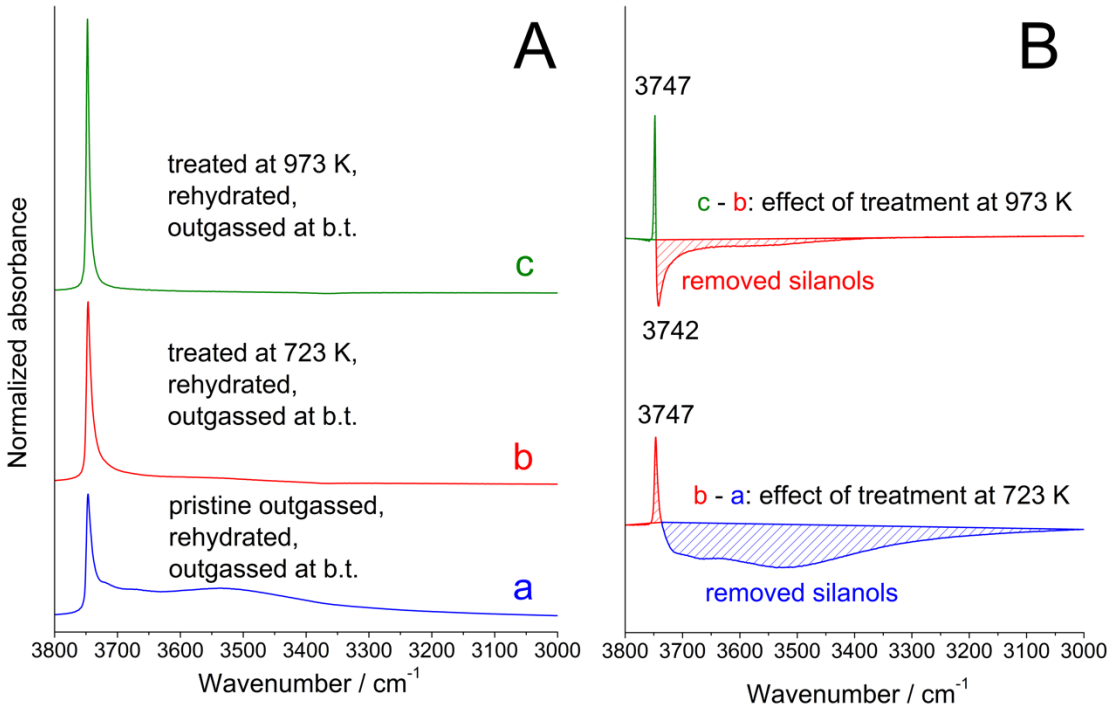

Figure 2. IR spectra of SiO_2 samples with different surface SiOH populations (spectra collected after outgassing at b.t.). Data in section A are the result of the subtraction of the ν(OH) pattern due to intraglobular silanols (inaccessible to reactants; curves b in Figure 1) from the total ν(OH) pattern (surface + intraglobular; curves a in Figure 1). a) pristine SiO_2; b) after calcination at 723 K; c) after calcination at 973 K. The differences between pairs of spectra in panel A are depicted in panel B, showing the decrease and increase in intensity of ν(OH) components due to surface Si-OH removed (negative signals) or affected by a change in intersilanol interaction (positive signal) as a consequence of the thermal treatments. Curve b-a) effect calcination at 732 K. Curve c-b) effect of the subsequent calcination at 973 K.

The much larger integrated intensity of the negative band in curve b-a with respect to the negative part of curve c-b does not correspond to the ratio of amounts of silanols removed by calcining at a different temperature. The same occurs for the positive sharp peak. In fact, the integrated intensity of OH stretching absorption increases linearly as the ν(OH) decreases, with a factor of ≈ 4 passing from H-bonded silanols absorbing at *ca.* 3530 cm^{-1} to very weakly interacting and isolated silanols absorbing in the 3730-3750 cm^{-1} range.[35-36]

Interaction of reactants with the silica surface

We initially considered methylamine (MA) and formic acid (FA) as reactants for amide bond (AB) formation because of the possibility to simplify quantum chemical calculations aimed to provide an atomistic interpretation of experiments (see below). Nevertheless, the expected product of the MA + FA condensation reaction (*i.e.*, presumably methyl formamide) was found to be poorly stable against hydrolysis (as from HR-MS analysis of an aqueous MFA solution, see Figure S2A of SI). Thus, the final step of the experimental procedure described in the following, requiring the contact with D_2O of the species remained on the silica surface, could result also in a

partial hydrolysis of methyl formamide. For this reason, 1-pentanamine (PA), with a longer alkyl chain likely protecting the amide-derivative from hydrolysis (see Figure S2B of SI) was also used. The spectra collected along the sequential admission of PA and FA on a silica sample are shown in the main text, while the analogous series obtained for MA and PA are reported in SI (Figure S3-S6 of SI), for the sake of completeness.

As a preliminary step, samples of thermally untreated silica were contacted in separated experiments with PA and FA vapors. The contributions of dispersive interactions between PA and the silica surface resulted in the resistance to outgassing at b.t. of a non-negligible fraction of adsorbed PA molecules (see Figure S7 of SI). Conversely, FA appeared to be reversibly adsorbed under outgassing at b.t. (Figure S3 of SI). These results were considered representative of the adsorptive behavior towards these molecules also for thermally treated SiO_2 samples, carrying at their surface fractions of the silanol population present on the pristine silica, and without the additional presence of reactive strained siloxane bridges, as commented above. Thus, the AB reaction between PA and FA was carried out, using the IR cell as a batch reactor, with the inlet for reactants on the top and the sample at the bottom (see Figure S8 of SI). SiO_2 samples were contacted first with PA vapors and outgassed at b.t., leaving adsorbed amine molecules, and then doses FA vapors at low pressure were sequentially admitted in the cell. The effect of the sequential admission of reactants on the thermally untreated SiO_2 samples, as monitored by IR spectroscopy, is displayed in Figure 3 and Figure 4. The admission of PA molecules results in a perturbation of the ν(OH) pattern of the surface silanols, and in particular the sharp component peaked at 3747 cm^{-1} is converted in a broad band at lower frequency spread over the 3300-2400 cm^{-1} range, indicating that SiOH behaves as a donor of a strong H-bond towards adsorbed amine molecules (Figure 3, curves a and b and Figure S7 of SI). In a first experiment, the subsequent

outgassing of PA was stopped when the narrow ν(OH) feature at high frequency started to reappear (Figure 3, curve b). The perturbation of the ν(OH) pattern is accompanied by the appearance signals at 3374 and 3311 cm^{-1} (asym and sym $\nu(NH_2)$, respectively), 3000-2800 cm^{-1} ($-CH_3$ and $-CH_2$ stretchings), 1605 cm^{-1} ($\delta(NH_2)$) and 1470 cm^{-1} (asym $\delta(CH_3)$).[37]

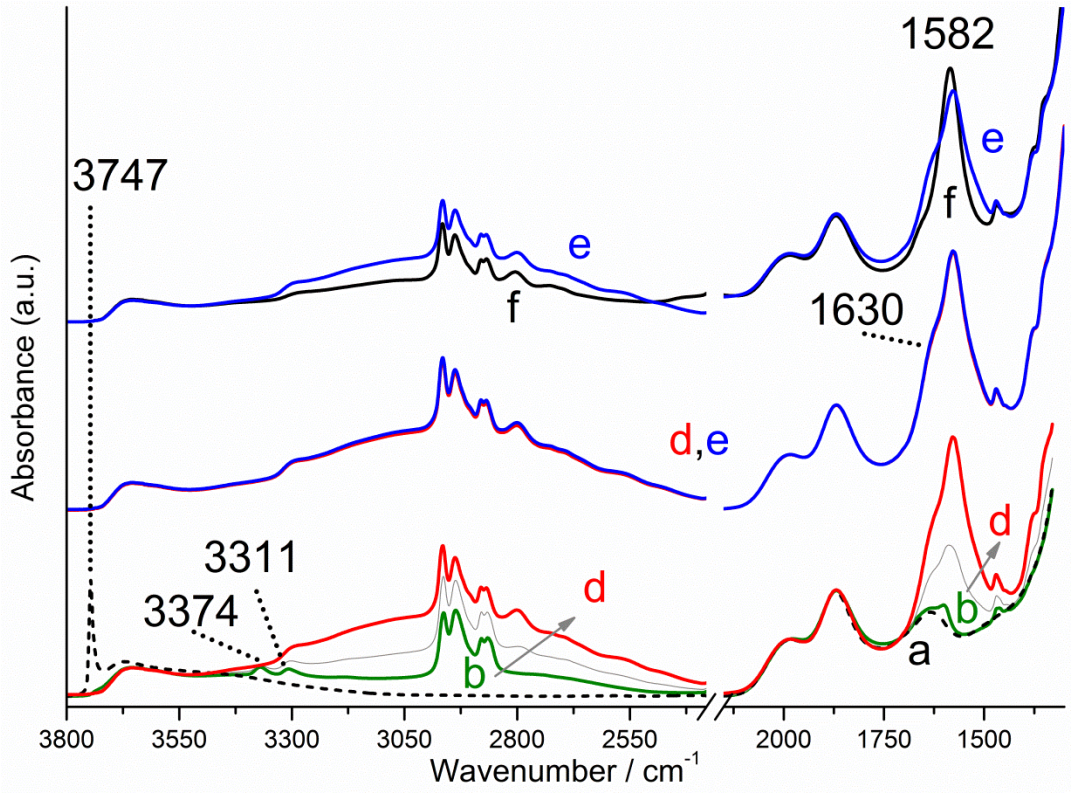

Figure 3. Infrared spectra of pristine SiO_2 outgassed at b.t. and subsequently contacted with 1 pentanamine (PA) and formic acid (FA): a) dotted black line, sample outgassed at b.t.; b) after admission of PA and subsequent outgassing until the initial reappearance of the narrow silanol ν(OH) peak high frequency ; b→d) after admission of FA until depletion of $\nu(NH_2)$ signals at 3374 and 3311 cm^{-1}; d, e) after subsequent outgassing at b.t.; f) after D_2O admission (20 mbar)/outgassing at b.t. until spectral invariance.

Increasing amounts of FA were then admitted on the silica sample in contact with PA, until depletion of the $\nu(NH_2)$ stretching signals (curves b→d). In parallel bands due to formate species (2815 cm^{-1}: $\nu(CH)$; 1575 cm^{-1}: asym $\nu(COO^-)$)[38] and to protonated PA (*ca*. 3300 cm^{-1}: $-NH_3^+$ stretchings; 1620 cm^{-1}(shoulder): mainly asym $\delta(NH_3^+)$, since the sym $\delta(NH_3^+)$ is likely contributing to the low frequency side of the asym $\nu(COO^-)$ band)[37] appear. If present, the $\nu(C=O)$ signal due to possibly formed amide molecules is expected to fall in the 1670-1650 cm^{-1} range, thus overlapped to the deformation band of the co-produced H_2O (see above) and the asym $\delta(NH_3^+)$ signal. To assess the presence or absence of a $\nu(C=O)$ sub-band, the sample was outgassed at b.t (curves d,e), and then underwent D_2O adsorption/desorption cycles (see above, Figure 1 and related comments), in order to downshift the signals due water and protonated amine groups, converted in ND_3^+ by isotopic exchange, leaving almost unperturbed only the $\nu(C=O)$ component, if present. This was not the case (curve f), indicating that amide molecules were not formed. An additional view of this result is shown in Figure 5, in comparison with those obtained by carrying out the PA-FA reaction in different conditions

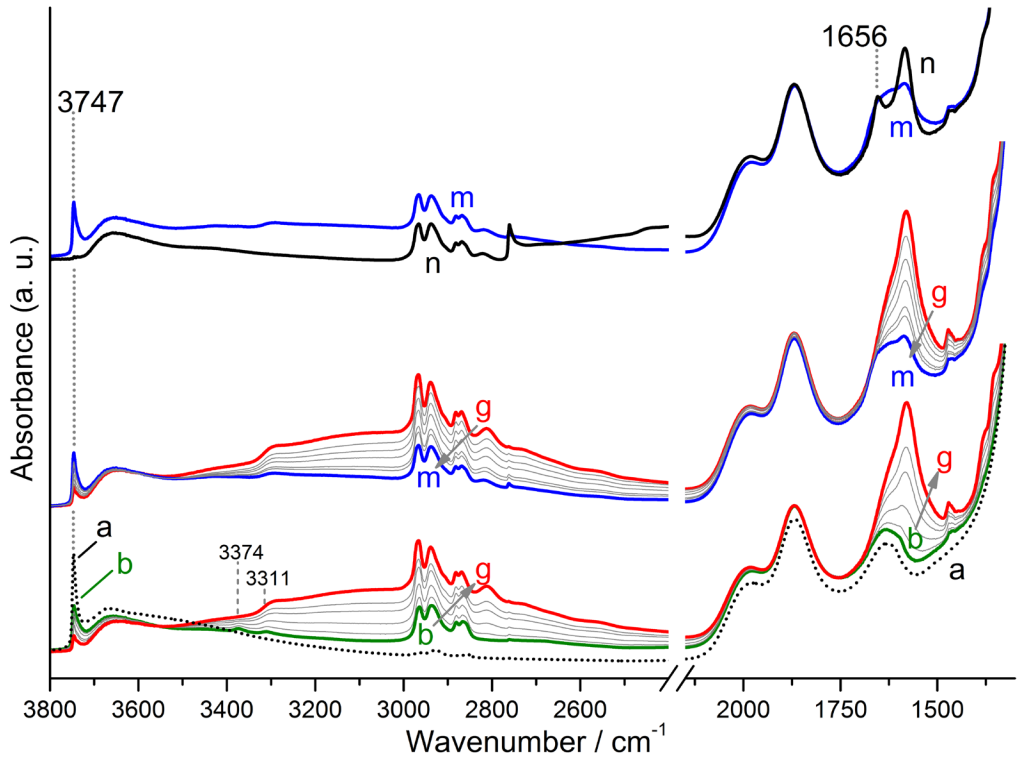

Figure 4. Infrared spectra of pristine SiO_2 outgassed at b.t. and subsequently contacted with 1 pentanamine (PA) and formic acid (FA): a) dotted black line, sample outgassed at b.t.; b) after admission of PA until halving the intensity of the peak at 3747 cm^{-1}, due to isolated silanols; b→g) after admission of FA until depletion of $\nu(NH_2)$ signals at 3374 and 3311 cm^{-1}, grey curves show intermediate amounts of FA; g→m) after subsequent outgassing at b.t. until invariance of spectra (grey curves show intermediates steps of outgassing); n) after D_2O admission (20 mbar)/outgassing at b.t. until spectral invariance.

The experiment was then repeated on a different silica pellet, this time prolonging the outgassing of initially adsorbed PA molecules in order to recover in a larger extent the high frequency ν(OH) signal of silanols (Figure 4, curves a,b). Thus, doses of FA were subsequentially admitted, with a consequent decrease in intensity of the ν(OH) band of unperturbed surface silanols (curves b→g). After subsequent outgassing (curves g→m), the isotopic exchange by

admission/outgassing of D_2O vapor was carried out, and in this case a band at 1656 cm^{-1}, assignable to the ν(C=O) of amide molecules is clearly detected (curve n).

IR data collected along equivalent experiments on silica samples calcined at 723 K and 973 K are reported in Figure S9 and S10 of SI.

Detection of reaction products

For the sake of clarity, the spectral features due to species remaining on the surface of pristine and calcined silica samples after the sequential contact with PA and FA, and the final H/D exchange are shown in panel A of Figure 5, focusing on the range relevant for the ν(C=O) band of amide species. For the sake of completeness, also the spectra obtained for the MA+FA reaction are reported in panel B of Figure 5 (original spectra in Figures S4-S6 of SI). As reported above, the ν(C=O) signal is absent in the spectrum resulting from the experiment carried out on thermally untreated silica loaded with PA molecules occupying all surface silanols (panel A, curve a_0). Conversely, this signal is present for experiments carried out by dosing FA on thermally untreated silica samples loaded with PA or MA molecules occupying only a fraction of surface silanols (curves a, panel A and B, respectively). As far as the effect of removal of surface silanols by thermal treatment of silica is concerned, data resulting from both the PA+FA and MA+FA sets of experiments show an equivalent trend: a ν(C=O) band at 1656/1665 cm^{-1} assignable to penthylformamide/methylformamide present when the catalyst is silica in the pristine form (curves a) and calcined at 723 K (curves b), whereas only traces of these signals appear for experiments carried out on silica calcined at 973 K (curves c). The resistance of penthylformamide towards hydrolysis allowed to confirm its formation by HR-MS analysis of the washing aqueous solution of samples contacted with PA and FA (panel A inset: m/z =

116.1069, and Figure S2 and S11 of SI). This collection of data clearly indicates that amidation between PA/MA and FA occurred on silica only in the presence of silanols responsible of the 3742 cm^{-1} peak, no longer present after calcination at 973 K (see Figure 2B). Furthermore, formation of ionic pairs from adsorbed PA and FA (as monitored through the $\nu_{asym}(COO^-)$ signal at 1584 cm^{-1} in panel A) also seems to depend on the presence of silanols characterized by the ν(OH) at 3742 cm^{-1}.

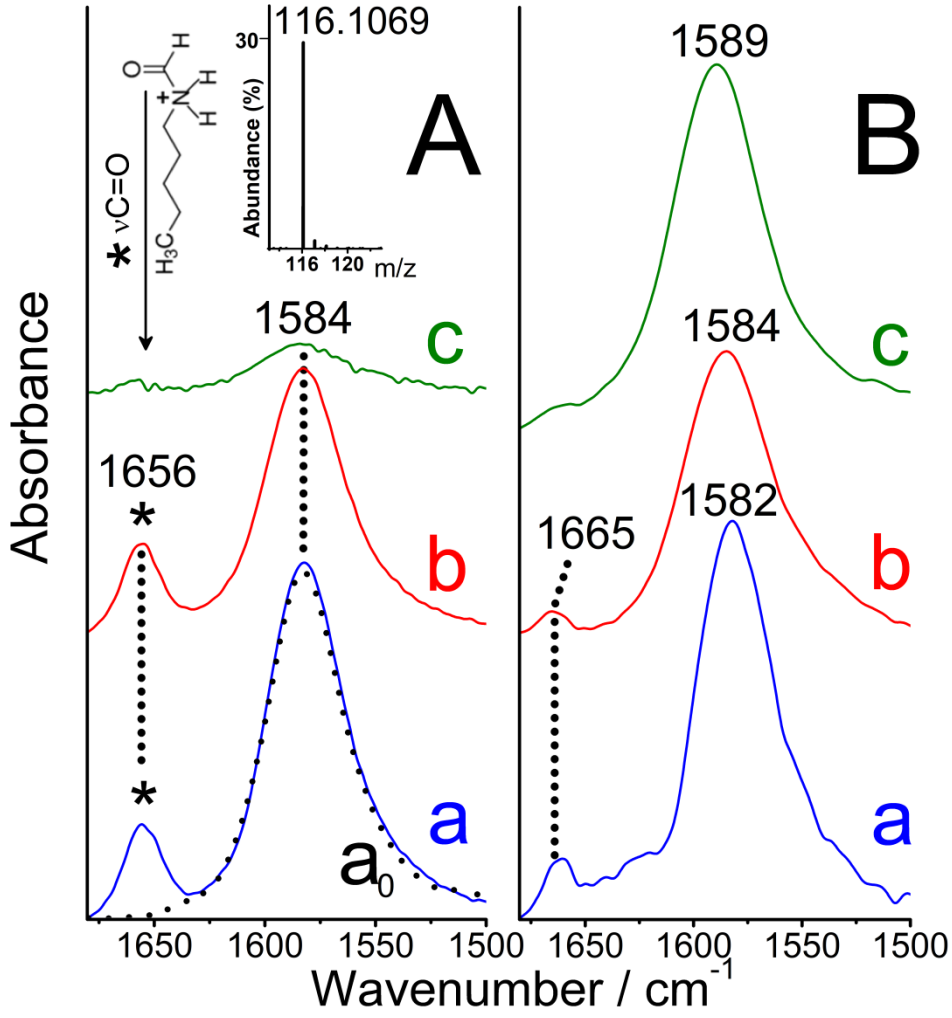

Figure 5. IR spectra, in the 1700-1500 cm^{-1} range, of species left adsorbed on the surface of SiO_2 samples after the sequential contact with PA + FA (panel A) or MA + FA (panel B). Curve a_0 (dotted line) in panel A is the result of the differences between the last and the first spectra in

Fig. 3 (curves f and a, respectively). The other curves are the results of the difference between the last and the first spectra in Figure 4, S9 and S10 (PA + FA reaction, panel A), and Figure S4-S6 (MA+FA reaction, panel B): a) pristine SiO_2; b) SiO_2 calcined at 723 K and at c) 973 K.

This was not the case of the MA+FA reaction (panel B, band at 1582-1589 cm^{-1}), where adsorbed amine molecules were in equilibrium with molecules in vapor phase (see comments on Figure S4-S6 in SI), and these latter underwent salification with incoming FA, irrespective of the hydroxylation state of the silica surface.

Rationalization of experimental results by means of quantum chemical calculations

Our experimental findings pose a fundamental question: why the presence of the specific SiOH peaked at 3742 cm^{-1} is mandatory for the occurrence of AB formation? Answering this question will indeed shed some light into the role of the silica surface in the reaction. To this end, we use quantum chemical calculations as they can provide an atomistic interpretation of the experiments. Calculations adopt a cluster approach within the ONIOM2[B3LYP/6-311++G(d,p):MNDO] method for optimization and frequency calculations and refining the energetics with single-point energy calculations at full B3LYP-D3/6-311++G(d,p) level, inclusive of dispersion interaction estimate. Further computational details are shown in the Methods section. The silica cluster model (shown in Figure 6A) presents two very weakly interacting SiOH groups, with a H···O and a O···O intersilanol distances of about 4.9 and 5.5 Å, respectively, as imposed by the rigidity of the model. It is worth noting that the four-Si-membered ring hosting the silanol pair did not play any specific role in the reaction, as it simply derives from the edingtonite mineral adopted to define the cluster model (see Computational details). Calculated ν(OH) frequencies (see Figure S12.A and Table S1 of SI) are 3746 and 3751

cm^{-1} (using a scaling factor of 0.959[39]); *i.e.*, exactly mimicking the frequency shift of 5 cm^{-1} of the experimental 3747 and 3742 cm^{-1} bands. Rotation of the SiOH groups to break the weak attractive through-space interaction equalizes the ν(OH) values, as expected (3751 and 3752 cm^{-1}, see Figure S12.B). These results indicate that the model reported in Figure 6A does account quantitatively for the measured spectroscopic features on the real silica sample outgassed at 723 K.

The adopted cluster model exhibits H atoms to cap the Si dangling bonds. In the real material, exposed surface tetrahedra exhibit OH groups as termination, which renders the material hydrophilic to various degrees. To check for the dependence of the results upon H or OH termination, we repeated some calculations for cluster terminated by OH groups. The optimized structural parameters of this cluster model are very similar to those in the H-saturated one, with the H···O and a O···O inter-silanol distances of about 5.0 and 5.6 Å (see Figure S13 of SI). The calculated ν(OH) frequencies of 3750 and 3745 cm^{-1} (using the 0.959 scaling factor) are very close to those for the H-saturated cluster with the same frequency shift of 5 cm^{-1} (see Table S2 of SI). In conclusion, details of the H-terminated cluster model adopted in this work are indistinguishable from the OH-terminated one.

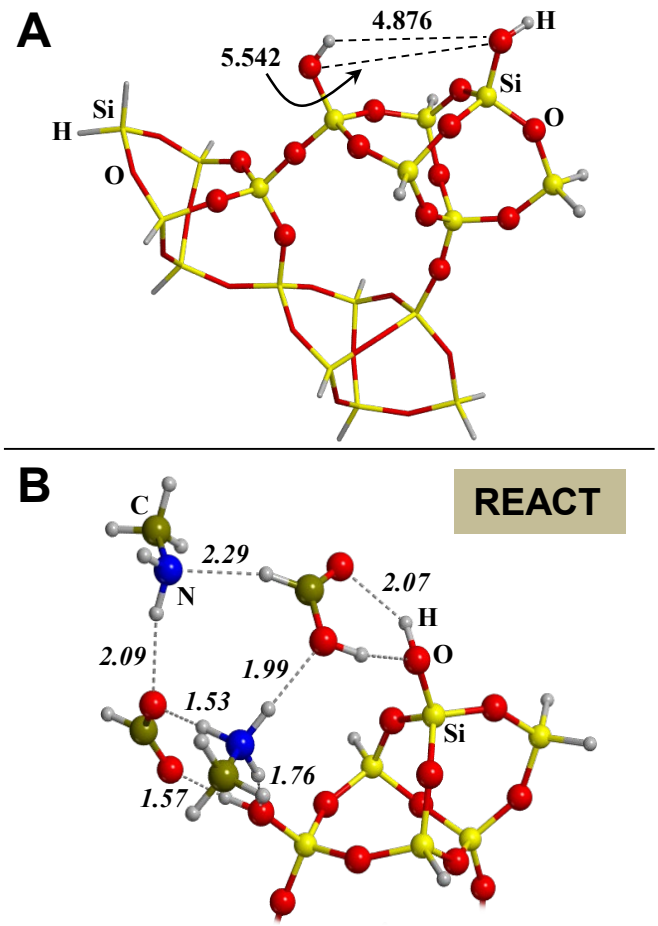

Figure 6. A) cluster model for the SiO_2 surface, where atoms in balls belong to the high-level zone and in sticks to the low-level zone in the ONIOM2 calculations. B) The pre-reactant structure, since now referred to as REACT, for AB formation, presenting ionic and canonical forms of the FA/MA pair. Only the reactive part is presented. Bond distances are in Å.

As mentioned above, to simplify the calculations, we adopted FA and MA as reactants to give methylformamide (MFA). Experimentally, salification is observed, meaning that $CH_3NH_3^+$/CH_3-$(CH_2)_4$-NH_3^+ and $HCOO^-$ are present. However, these ionic species are not reactive towards AB formation since neither the amino groups can carry out the nucleophilic attack (they are in the ammonium cationic form) nor the C of the carboxylic groups are electrophilic enough (they are in the form of carboxylate). This is at variance with the canonical

pairs, which are indeed prone towards AB formation. Since the experimental results indicate that amide bond formation actually occurs, there must be a co-presence of ionic and canonical pairs, the latter feeding the reaction channel giving the amide product. Thus, a suitable initial state for the reaction is REACT, shown in Figure 6B, in which two FA and two MA interact with the silica sites, with one FA/MA pair in ionic form and the other as canonical pair. It is worth noting that forcing REACT towards a structure (ION, Figure S14) in which all pairs are set up to be in the ionic state, brings about an increase in the free energy by about 5 kcal mol^{-1} (Table S3 of SI), with only one SiOH engaged in the interaction. When all SiOH groups are occupied like the one in ION, we end up with only ion pairs at the surface, in agreement with FA interacting with an initially PA loaded silica surface (see Figure 3 and related comments). While REACT may bring to AB formation, ION like structures are obviously inactive (*see supra*).

Figure 7A shows the proposed mechanism for the AB formation alongside the corresponding free energy profile at 323 K, as we considered that the reaction occurs under the thermal effect of the infrared beam. Potential energy values and free energy values at 298 K are available in Figure S15 and Table S4 of SI. The canonical forms of MA and FA of the initial state (the REACT structure of Figure 6B) react through a C-N coupling (TS1) to form the metastable $CH_3NH_2(+)CHOHO(-)$ zwitterionic species (INT). The calculated free energy barrier at 323 K ($\Delta G^{\neq}_{323}$) of this coupling is 11.5 kcal mol^{-1}, with INT at 9.6 kcal mol^{-1} with respect to REACT. The second step involves the dehydration and final formation of MFA. It takes place by two simultaneous processes (TS2): i) a proton transfer from $CH_3NH_3^+$ to the OH group of INT to release H_2O; and ii) a proton transfer from the NH_2 moiety of the metastable species to the deprotonated $HCOO^-$. This step has an intrinsic $\Delta G^{\neq}_{323}$ of 18.5 kcal mol^{-1} and the overall process is favorable by -7.8 kcal mol^{-1} (see PROD-n). Interestingly, the initial ionic FA/MA pair

transforms into a canonical pair after AB condensation (see PROD-n). An interesting point is to assess whether this canonical pair can be converted back to the ion pair, restoring its catalytic activity for a new condensation cycle. This process is shown in Figure 7B: FA transfers its proton to MA, which moreover is assisted by the H_2O molecule resulting from the AB condensation. The calculated intrinsic $\Delta G^{\neq}_{298}$ is very low (1.2 kcal mol^{-1}, TS3) and the final state is more stable by 1.3 kcal mol^{-1} (PROD-i).

The proposed mechanism clearly shows that silica surface is essential for the occurrence of the AB formation, as the uncatalyzed gas-phase AB process proceeds in a concerted way with a high kinetic barrier of $\Delta G^{\neq}_{323} \approx 48$ kcal mol^{-1} (see Figure S16 and Table S5 of SI). The key point is the presence of the spatially specific SiOH surface sites, allowing the coexistence of FA/MA pairs in their ionic and canonical states. The FA/MA ion pair actively participates in the AB formation between the FA/MA canonical pair, particularly in the dehydration step, in which the acidity of $CH_3NH_3^+$ lowers the energy barrier for the H_2O elimination. Remarkably, the removal of one silanol group from our model cluster leads to the transformation of the canonical FA/MA pair into its ionic form, which is stabilized by the interaction with the other FA/MA ion pair (see Figure 8) *de facto* preventing the nucleophilic step essential for the AB formation. Thus, the presence of only isolated surface SiOH does not provide a suitable scenario for the AB formation, in full agreement with the spectroscopic evidence provided by Figure 5A, B, curves c for the silica sample outgassed at 973 K

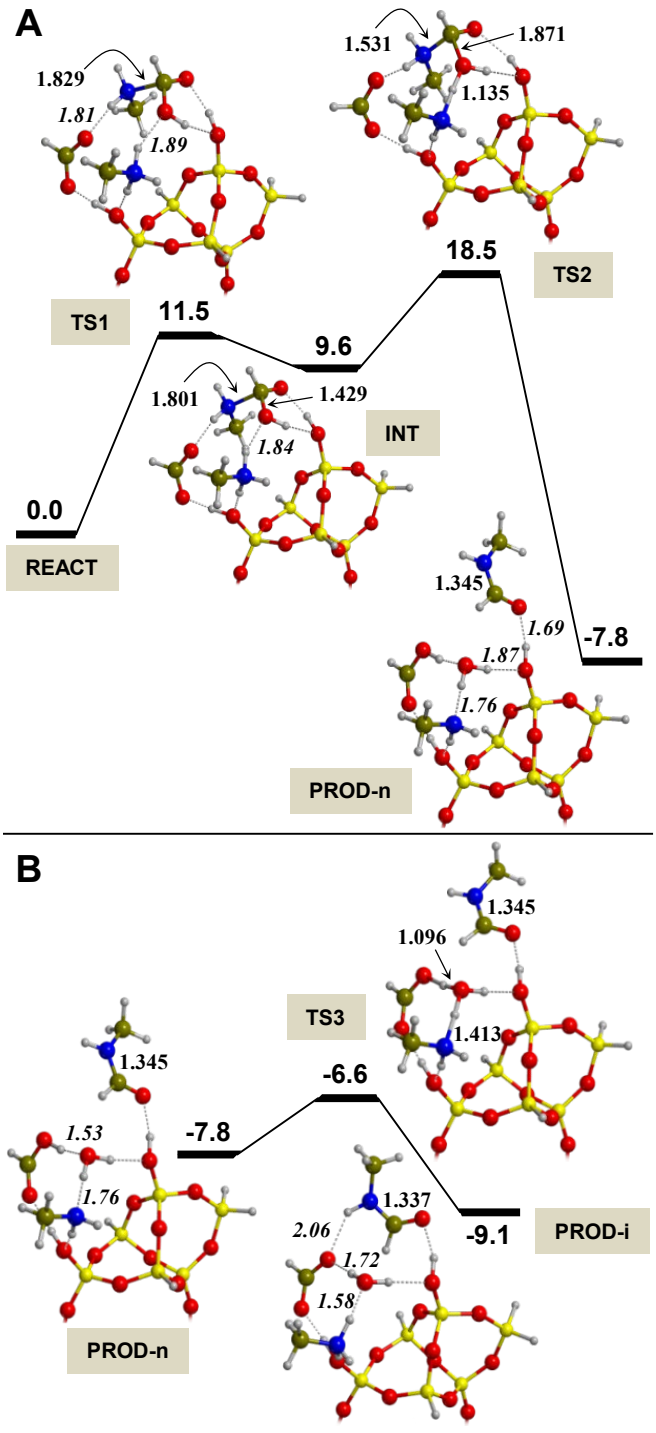

Figure 7. Free energy profiles at 323 K (in kcal mol^{-1}) for the AB formation mechanism (A) and the restoring of the ionic FA/MA pair (B). Bond distances are in Å.

It can be then proposed that the actual reaction is between canonical FA and MA in the presence of the ionic $CH_3NH_3^+/HCOO^-$ pair, in which the role of the weakly interacting silanol groups is essentially to help setting up the coexistence of both canonical and ionic pairs. The silanol groups, in fact, are not directly involved in making/breaking bonds during the catalytic process. Noteworthy, this can be compared with the role of solid state surfaces in heterogeneous catalytic processes carried out by frustrated Lewis pairs (FLP). In these cases, surfaces are simply used to immobilize the FLP, while the actual catalysis is performed by the supported Lewis acid/base components of the FLP.[40-42] Nevertheless, in our case the difference is that one of the two SiOH of the weakly interacting pair acts as an anchoring site for surface bound $CH_3NH_3^+/HCOO^-$ pair which is the actual catalyst in the dehydration step, and the other acts as an anchoring site for the reactant; *i.e.*, the canonical CH_3NH_2/HCOOH pair.

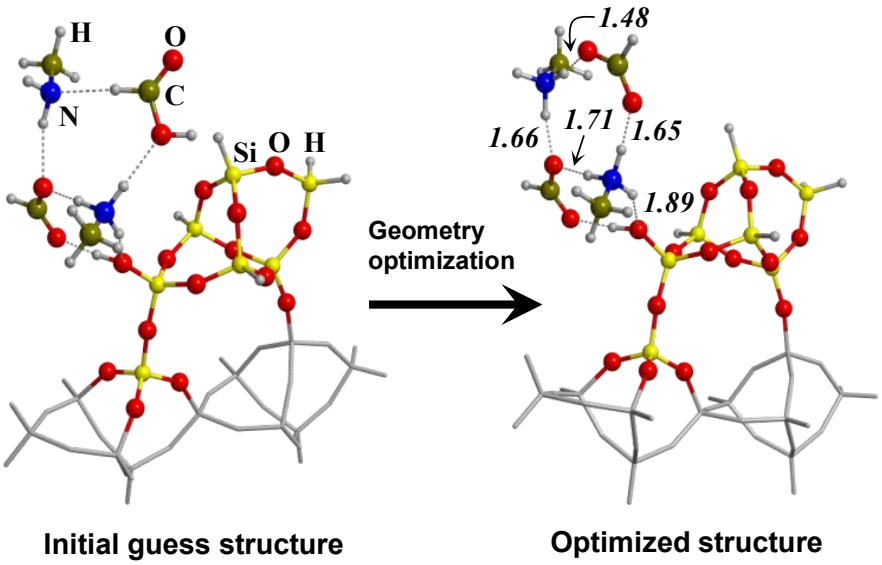

Figure 8. ONIOM2-optimized geometry (H-bond distances in Å) of a system with 2 formic acids and 2 methylamines on a silica surface model with only one SiOH group. The initial guess structure is REACT in which one SiOH group was removed.

Moreover, the interaction of the canonical FA with both SiOH and the $CH_3NH_3^+$ species activates the C atom of the C=O group towards the nucleophilic attack, as shown by the formation of the metastable $CH_3NH_2(+)CHOHO(-)$ species (INT in Figure 7A). Remarkably, formation of this kind of metastable intermediates was also identified in simulations on the peptide bond formation in the ribosome,[43] which induces a lowering of the energy barriers compared to the uncatalyzed processes. The stabilization of these metastable species, in our case, is due to the interaction with one silica SiOH group and the FA/MA ion pair adsorbed on the other SiOH, whereas in the ribosome a sugar OH functionality and a water molecule play this role.

The experimental set up available and the reaction procedure adopted (a series of small doses of FA admitted on preadsorbed PA) prevented the possibility to obtain experimental insights on the kinetic features of the reaction. However, by adopting the standard transition state theory using the DFT data for the potential free energy surface of the AB reaction (see Figure 7A) allows to derive the kinetic constants for each reaction step, as highlighted in Scheme 1. Results are: k_1 = 1.11×10^5 s^{-1}, k_{-1} = 3.48×10^{11} s^{-1}, k_2 = 5.46×10^6 s^{-1}, K = 3.19×10^{-7} and k = 1.74 s^{-1}, with (by assuming first-order in the REACT adduct) a half-life time of $\tau_{1/2}$ = 0.2 s.

$$\text{REACT} \underset{k_{-1}}{\overset{k_1}{\rightleftharpoons}} \text{INT} \xrightarrow{k_2} \text{PROD-n}$$

$$\frac{d[\text{PROD}-\text{n}]}{dt} = k[\text{REACT}] = K\times k_2\,[\text{REACT}];\; K = \frac{k_1}{k_{-1}}$$

Scheme 1. Kinetic model adopted to derive rate constants for the AB formation.

From amorphous silica to α-quartz: relevance in prebiotic chemistry

While the present results are fully valid for technological applications, it is stimulating to consider how to put them in the prebiotic context due to the absence of amorphous silica as natural material. In nature, silica is present in its crystalline polymorphs, mainly α-quartz or β-cristobalite. The question is, therefore, whether the presence of the specific silanol pair responsible of the stabilization of the ion/canonical reactive species is exclusive of a specifically treated amorphous silica material. To elucidate this aspect, we have studied the occurrence of specific surface SiOH pairs at the α-quartz hydroxylated (010) surface, one of the most common crystal faces of α-quartz. This surface has a surface OH density of 7.4 OH nm^{-2} and has been exhaustively characterized theoretically by some of us.[44] Due to the high degree of hydroxylation, most of the silanol groups are H-bonded so that the pristine surface does not exhibit the specific SiOH non-interacting pairs (see "pristine surface" of Figure 9A). However, mutually interacting silanol groups can undergo condensation reactions yielding the formation of siloxane groups; *i.e.*, SiOH + SiOH → Si-O-Si + H_2O, a process quite common on such a highly hydroxylated surface. Hence, "defects" are created in the silanol population of an ideally perfect crystalline surface.

We have easily identified condensation processes (between those silanol pairs present in the insets of Figure 9A) giving rise to a pair of silanols no longer involved in H-bonding (labeled with an asterisk in Figure 9A). We optimized at B3LYP/6-311G(d,p) level with the

CRYSTAL14 program[45] the surface structure upon condensation of these silanol groups. The resulting surface (see the top and lateral view of the "condensed surface" in Figure 9A and Figure 9B, respectively) exhibits the specific SiOH pair with H···O and O···O inter-silanol distances (about 5.0 and 5.6 Å, respectively), very close to those for the cluster model adopted here. Moreover, the calculated ν(OH) frequencies for the SiOH pair are 3737 and 3733 cm^{-1}, with a frequency difference almost coincident with that recorded experimentally (*i.e.*, 5 cm^{-1}). Additionally, to determine if the condensed α-quartz surface can host the ion/canonical reaction species, we have optimized the REACT structure on top of the (010) α-quartz surface to assess its structural stability. The optimized structure (see REACT-analogue of Figure 9B) shows a structure exhibiting the same H-bond patterns as those computed for the cluster model.

It is reasonable, however, wondering if the formation of the specific weakly interacting silanol pair via condensation of silanol groups is exclusive to the α-quartz (010) surface or is common also for other hydroxylated surfaces. For this reason, we extended the condensation processes to other α-quartz hydroxylated surfaces; namely, the (001), the (011) and the (100) ones, to see whether the resulting surfaces also present the specific weakly interacting silanol pair. Results indicate that this is indeed the case for most of them. These pairs of silanol groups are separated by about 4.6 – 5.0 Å, while frequency calculations revealed frequency difference of about 5 – 8 cm^{-1} (see Figure S17-S19 of SI).

In view of these results, we argue that other common silica forms with moderate degree of surface hydroxylation can exhibit similar catalytic activity towards the AB formation to that occurring on our amorphous silica sample.

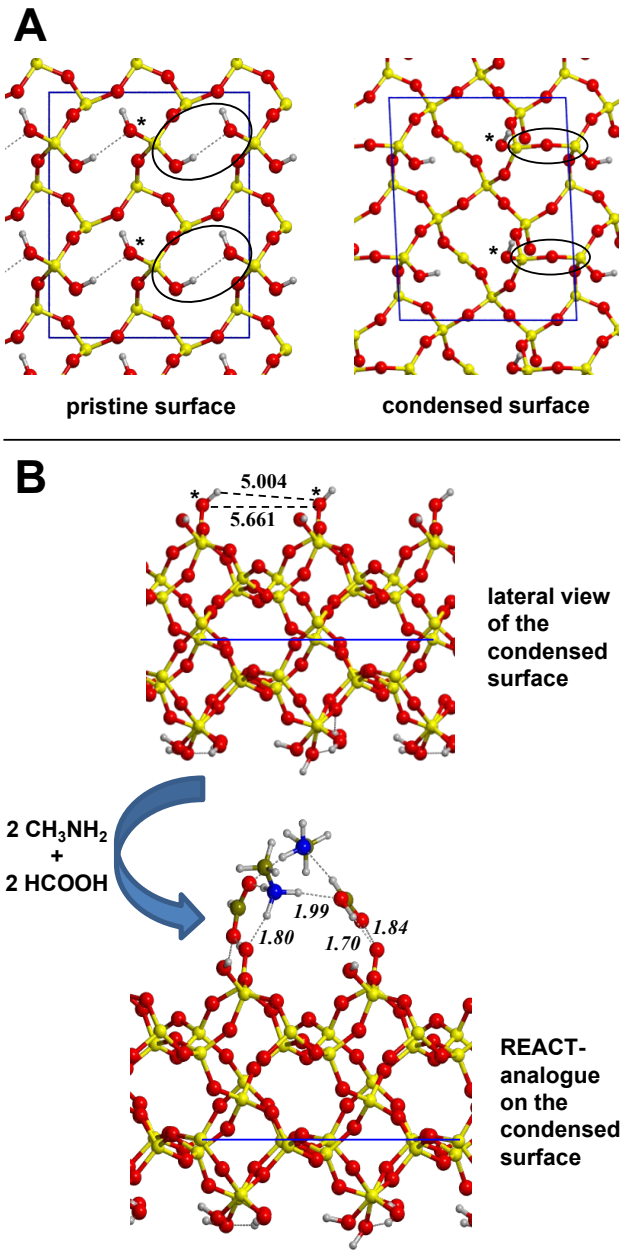

Figure 9. A) Top view of the crystalline (010) α-quartz surface in its pristine and condensed forms. The SiOH groups labelled by asterisk are those constituting the specific SiOH pair while the insets show the condensing silanols and the resulting siloxane groups. B) Lateral view of the optimized geometry of the condensed (010) α-quartz surface (above), and optimized structure of the pre-reactant complex for AB formation (that is, the REACT-analogue) on the condensed (010) α-quartz surface, presenting the ionic and canonical forms of the FA/MA pairs (below). Bond distances are in Å. Unit cell borders are highlighted in blue.

CONCLUSIONS

This work focuses on the direct amide bond formation between amines and carboxylic acids occurring on silica surfaces by combining IR measurements and quantum chemical calculations based on established accurate model chemistry. IR results indicate that AB formation occurs only if specific weakly interacting SiOH pairs are present. The amount of these pairs depends on the "thermal history" of the material. In the present case, we adopted a pyrogenic silica with an initial low silanol density (*ca*. 1.5 OH nm^{-2}). We proved that thermal treatment at 973 K almost depletes the active pairs. Quantum chemical calculations provided the atomistic model for this SiOH pairs, which in turn are responsible, as absorbing site, of the coexistence of amine/carboxylic acid pairs in their canonical and ionic forms. This coexistence is an essential point for the occurrence of the AB formation, as the canonical pair is the reacting one while the ion pair acts as catalyst for the dehydration step. Moreover, the interaction of the canonical pair with both surface SiOH and the ion pair stabilizes a metastable intermediate species, inferring a significant decrease of the overall energetics compared to the uncatalyzed gas-phase process. Standard transition state theory on the DFT free energy barriers indicates that the kinetic of our silica-catalyzed mechanistic proposal for the AB formation is reasonably fast. The work also points out that the presence of the specific SiOH group pairs is not exclusive of the adopted SiO_2 sample, but they can also be present in other types of silicas with moderate surface silanols populations. This might be also the case of natural common forms of silica polymorphs present in early Earth, so that they may have behaved as a cradle for the prebiotic amide bond formation.

METHODS

Experimental Details

The commercial silica powder AEROSIL® OX50 (by EVONIK; SiO_2 content ≥99.8 wt%, as from www.aerosil.com) was used as catalyst. Formic acid, 1-pentanamine and D_2O (99.90% D) were high-purity Sigma-Aldrich products. The vapors of these chemicals, as well as those of Milli-Q water (Millipore system), were admitted onto the samples in the IR cell after several freeze-pump-thaw cycles. Pure gas N-methylamine was purchased from PRAXAIR (UCAR).

The thermal treatments of the samples were carried out in a muffle furnace. SiO_2 powder was pressed in form of self-supporting pellets which were introduced in the furnace and ramped for 30 min up to 723 K and kept at this temperature for 2.5 hours. Samples were then left to cool down to room temperature (required time *ca*. 5 hours). A set of so treated pellets was then ramped for 30 min up to 973 K, again kept at this temperature for 2.5 hours, and left to cool down to room temperature (required time *ca*. 9 hours).

Volumetric measurements of the specific surface area (N_2 adsorption at 77 K; BET method) were carried out on pieces obtained by manual crushing in mortar pellets of the pristine silica or resulting from the thermal treatments. The instrument used was an ASAP2020 by Micromeritics. Before measurements, samples were outgassed overnight at room temperature (residual pressure: 10^{-4} mbar).

For IR spectroscopic measurements, pellets of the pristine silica or resulting from the thermal treatments described above were placed in a traditional IR cell equipped with CaF_2 windows and a valve for connection to vacuum lines (residual pressure $1.0 \cdot 10^{-5}$ mbar) allowing adsorption/desorption experiments to be carried out in situ. The spectra were collected with a Bruker VECTOR22 instrument (DTGS detector) at beam temperature (*ca*. 323 K) with a resolution of 4 cm^{-1}, by accumulating 100 scans, to attain a good signal-to-noise ratio.

After experiments involving the contact of both reactants (amines and formic acid) with the samples, pellets were removed from the cell, manually ground in an agate mortar and suspended in 0.5 mL of Milli-Q water. Suspensions were shaken for 15 min by a Vortex mixer and then centrifuged for 10 min at 10k rpm. After removal of the supernatant, the solid was treated a second time with the same volume of water. The two aliquots of the aqueous solutions were then mixed, and analyzed by high-resolution mass spectrometry.

High-resolution mass spectrometry analyses of the washing solutions were performed using an LTQ Orbitrap mass spectrometer (Thermo Scientific) equipped with an atmospheric pressure interface and an electrospray ionization (ESI) source. The source voltage was set to 4.48 kV. The heated capillary temperature was maintained at 538 K. The tuning parameters adopted for the ESI source were: capillary voltage 0.02 V, tube lens 24.77 V; for ions optics: multipole 0 offset −4.28 V, lens 0 voltage −4.36 V, multipole 0 offset −4.28 V, lens 1 voltage −13.69 V, gate lens voltage −8.84 V, multipole 1 offset −18.69 V, front lens voltage −5.09 V. Mass accuracy of recorded ions (vs calculated) was ± 1 mmu (without internal calibration). Samples, added of 100 μL of a 0.1 M HCOOH aqueous solution, were delivered directly to the mass spectrometer via a hamilton microliter syringe at constant flow (10 μl min^{-1}).

Computational Details

Calculations were run on a cluster model to simulate a silanol-containing amorphous silica surface (shown in Figure 6A). The cluster was derived from a secondary building unit of the crystalline all-silica edingtonite structure to ensure sufficient rigidity in the models during geometry optimization as envisaged by the presence of four-Si-membered rings in the framework.

All molecular calculations were performed using the Gaussian 09 program.[46] To increase the speed of the calculations, the structures of the reactants, transition states, and products were optimized using the ONIOM2[B3LYP/6-311++G-(d,p):MNDO][47-50] method, where atoms in balls belong to the high-level zone and in sticks to the low-level zone (see Figure 6A). For consistency, reactant molecules were included in the high-level zone of the ONIOM2 calculations. The reaction energetics were refined by performing full B3LYP-D3/6-311++G(d,p) single-point energy calculations on the optimized ONIOM2 stationary points, with dispersion interactions taken into account by including the Grimme's D3 correction term.[51] Structures were characterized by the analytical calculation of the harmonic frequencies as minima (reactants and products) and saddle points (transition states). Free energies were computed including enthalpy and entropy contributions obtained at the ONIOM2 level to the B3LYP-D3/6-311++G(d,p)//ONIOM2 energies resulting from the standard rigid-rotor/harmonic-oscillator treatment.[52] In order to check the accuracy of the adopted theoretical level, the un-catalyzed gas-phase process has also been calculated at the CCSD(T)/aug-cc-pVTZ level on the ONIOM2 geometries. Comparison of the energetics between the two methods indicates that they are in very good agreement (data available in Table S5 of SI), thus supporting the suitability of the employed methodology.

Calculations based on crystalline models of α-quartz surfaces were performed using the periodic ab initio CRYSTAL14 code[45] For these calculations, we used the B3LYP density functional method and the all electron Gaussian 6-311G(d,p) standard basis set.

SUPPORTING INFORMATION

The Supporting Information is available free of charge on the ACS Publications website.

Supplementary experimental results: XRD patterns and Raman spectra of the SiO_2 powder, scheme of the cell used for the in-situ IR measurements, additional IR spectra of silica samples outgassed, contacted with methylamine/pentanamine or formic acid, and contacted with methylamine/pentanamine with formic acid, and HR-MS spectra of methylformamide and N-pentylformamide.

Supplementary computational results: optimized geometries and related energetic data of: i) different conformers of the silica cluster model, ii) H-saturated an OH-saturated silica cluster models, iii) the REACT structure with a silica cluster model containing two and one SiOH surface group, iv) the uncatalyzed gas –phase reaction of $CH_3NH_2 + HCOOH \rightarrow CH_3NHCHO + H_2O$, and v) pristine and condensed (001), (011) and (100) α-quartz surfaces; Cartesian and fraction coordinates of all the optimized structures.

ACKNOWLEDGMENTS

This work was supported by: MICINN (CTQ2014-59544-P, CTQ2014-60119-P and CTQ2017-89132-P), DIUE (projects 2014SGR482 and 2017SGR1320), 2011 ICREA Award, Catalonia Supercomputer Centre (CESCA), University of Torino (Ricerca Locale 2015) and by the Italian MIUR (Ministero dell'Istruzione, dell'Università della Ricerca) and from Scuola Normale Superiore (project PRIN 2015, STARS in the CAOS - Simulation Tools for Astrochemical Reactivity and Spectroscopy in the Cyberinfrastructure for Astrochemical Organic Species, cod. 2015F59J3R). AR is indebted to "Programa Banco de Santander" for a UAB distinguished

postdoctoral research contract and to “Ramón y Cajal” program. Dr. Marco Pazzi of the University of Torino is acknowledged for collecting HR-MS data.

REFERENCES

1. Pattabiraman, V. R.; Bode, J. W., Rethinking Amide Bond Synthesis. *Nature* **2011,** *480*, 471-479.
2. Constable, D. J. C.; Dunn, P. J.; Hayler, J. D.; Humphrey, G. R.; Leazer, J. J. L.; Linderman, R. J.; Lorenz, K.; Manley, J.; Pearlman, B. A.; Wells, A.; Zaks, A.; Zhang, T. Y., Key Green Chemistry Research Areas - A Perspective from Pharmaceutical Manufacturers. *Green Chem.* **2007,** *9*, 411-420.
3. Allen, C. L.; Williams, J. M. J., Metal-Catalysed Approaches to Amide Bond Formation. *Chem. Soc. Rev.* **2011,** *40*, 3405-3415.
4. Krause, T.; Baader, S.; Erb, B.; Gooßen, L. J., Atom-Economic Catalytic Amide Synthesis from Amines and Carboxylic Scids Activated In Situ with Acetylenes. *Nature* **2016,** *7*, 11732.
5. de Figueiredo, R. M.; Suppo, J.-S.; Campagne, J.-M., Nonclassical Routes for Amide Bond Formation. *Chem. Rev.* **2016,** *116*, 12029-12122.
6. Lundberg, H.; Adolfsson, H., Hafnium-Catalyzed Direct Amide Formation at Room Temperature. *ACS Catal.* **2015,** *5*, 3271-3277.
7. Liu, H. X.; Zhao, L. Y.; Yuan, Y. F.; Xu, Z. F.; Chen, K.; Qiu, S. X.; Tan, H. B., Potassium Thioacids Mediated Selective Amide and Peptide Constructions Enabled by Visible Light Photoredox Catalysis. *ACS Catal.* **2016,** *6*, 1732-1736.
8. Soulé, J.-F.; Miyamura, H.; Kobayashi, S., Powerful Amide Synthesis from Alcohols and Amines under Aerobic Conditions Catalyzed by Gold or Gold/Iron, -Nickel or -Cobalt Nanoparticles. *J. Am. Chem. Soc.* **2011,** *133*, 18550-18553.
9. Comerford, J. W.; Clark, J. H.; Macquarrie, D. J.; Breeden, S. W., Clean, Reusable and Low Cost Heterogeneous Catalyst for Amide Synthesis. *Chem. Commun.* **2009**, 2562-2564.
10. Calcio Gaudino, E.; Carnaroglio, D.; Nunes, M. A. G.; Schmidt, L.; Flores, E. M. M.; Deiana, C.; Sakhno, Y.; Martra, G.; Cravotto, G., Fast TiO_2-Catalyzed Direct Amidation of Neat Carboxylic Acids under Mild Dielectric Heating. *Catal. Sci. Technol.* **2014,** *4*, 1395-1399.
11. Hosseini-Sarvari, M.; Sharghi, H., ZnO as a New Catalyst for N-Formylation of Amines under Solvent-Free Conditions. *J. Org. Chem.* **2006,** *71*, 6652-6654.
12. Guo, C.; Jordan, J. S.; Yarger, J. L.; Holland, G. P., Highly Efficient Fumed Silica Nanoparticles for Peptide Bond Formation: Converting Alanine to Alanine Anhydride. *ACS Appl. Mater. Interfaces* **2017,** *9*, 17653-17661.
13. Lundberg, H.; Tinnis, F.; Zhang, J.; Algarra, A. G.; Himo, F.; Adolfsson, H., Mechanistic Elucidation of Zirconium-Catalyzed Direct Amidation. *J. Am. Chem. Soc.* **2017,** *139*, 2286-2295.
14. Bernal, J. D., The Physical Basis of Life. *Proc. Phys. Soc., London, Sect. B* **1949,** *62*, 597-618.
15. Smith, J. V., Biochemical Evolution. I. Polymerization on Internal, Organophilic Silica Surfaces of Dealuminated Zeolites and Feldspars. *Proc. Natl. Acad. Sci. USA* **1998,** *95*, 3370-3375.
16. Orgel, L. E., Polymerization on the Rocks: Theoretical Introduction. *Origins Life Evol. Biosphere* **1998,** *28*, 227-234.

17. Lahav, N.; White, D.; Chang, S., Peptide Formation in the Prebiotic Era: Thermal Condensation of Glycine in Fluctuating Clay Environments. *Science* **1978,** *201*, 67-69.
18. Ferris, J. P.; Hill, A. R.; Liu, R.; Orgel, L. E., Synthesis of Long Prebiotic Oligomers on Mineral Surfaces. *Nature* **1996,** *381*, 59-61.
19. Martra, G.; Deiana, C.; Sakhno, Y.; Barberis, I.; Fabbiani, M.; Pazzi, M.; Vincenti, M., The Formation and Self-Assembly of Long Prebiotic Oligomers Produced by the Condensation of Unactivated Amino Acids on Oxide Surfaces. *Angew. Chem. Int. Ed.* **2014,** *53*, 4671-4674.
20. Meng, M.; Stievano, L.; Lambert, J.-F., Adsorption and Thermal Condensation Mechanisms of Amino Acids on Oxide Supports. 1. Glycine on Silica. *Langmuir* **2004,** *20*, 914-923.
21. Lopes, I.; Piao, L.; Stievano, L.; Lambert, J.-F., Adsorption of Amino Acids on Oxide Supports: A Solid-State NMR Study of Glycine Adsorption on Silica and Alumina. *J. Phys. Chem. C* **2009,** *113*, 18163-18172.
22. Lambert, J.-F.; Jaber, M.; Georgelin, T.; Stievano, L., A Comparative Study of the Catalysis of Peptide Bond Formation by Oxide Surfaces. *Phys. Chem. Chem. Phys.* **2013,** *15*, 13371-13380.
23. Rimola, A.; Sodupe, M.; Ugliengo, P., Aluminosilicate Surfaces as Promoters for Peptide Bond Formation: An Assessment of Bernal's Hypothesis by ab Initio Methods. *J. Am. Chem. Soc.* **2007,** *129*, 8333-8344.
24. Schreiner, E.; Nair, N. N.; Wittekindt, C.; Marx, D., Peptide Synthesis in Aqueous Environments: The Role of Extreme Conditions and Pyrite Mineral Surfaces on Formation and Hydrolysis of Peptides. *J. Am. Chem. Soc.* **2011,** *133*, 8216-8226.
25. Phuakkong, O.; Bobuatong, K.; Pantu, P.; Boekfa, B.; Probst, M.; Limtrakul, J., Glycine Peptide Bond Formation Catalyzed by Faujasite. *ChemPhysChem* **2011,** *12*, 2160-2168.
26. Zaia, M. D. A., A Review of Adsorption of Amino Acids on Minerals: Was it Important for Origin of Life? *Amino Acids* **2004,** *27*, 113-118.
27. Lambert, J.-F., Adsorption and Polymerization of Amino Acids on Mineral Surfaces: A Review. *Origins Life Evol. Biosphere* **2008,** *38*, 211-242.
28. Román-Leshkov, Y.; Davis, M. E., Activation of Carbonyl-Containing Molecules with Solid Lewis Acids in Aqueous Media. *ACS Catal.* **2011,** *1*, 1566-1580.
29. Rimola, A.; Costa, D.; Sodupe, M.; Lambert, J.-F.; Ugliengo, P., Silica Surface Features and Their Role in the Adsorption of Biomolecules: Computational Modeling and Experiments. *Chem. Rev.* **2013,** *113*, 4216-4313.
30. Mitchell, A. R., Bruce Merrifield and Solid-Phase Peptide Synthesis: A Historical Assessment. *Pept. Sci.* **2008,** *90*, 175-184.
31. Muller, A. W. J.; Schulze-Makuch, D., Sorption Heat Engines: Simple Inanimate Negative Entropy Generators. *Physica A Stat. Mech. Appl.* **2006,** *362*, 369-381.
32. Akouche, M.; Jaber, M.; Maurel, M.-C.; Lambert, J.-F.; Georgelin, T., Phosphoribosyl Pyrophosphate: A Molecular Vestige of the Origin of Life on Minerals. *Angew. Chem. Int. Ed.* **2017,** *56*, 7920-7923.
33. Rimola, A.; Ugliengo, P.; Sodupe, M., Strained Ring Motif at Silica Surfaces: A Quantum Mechanical Study of their Reactivity towards Protic Molecules. *Comput. Theor. Chem.* **2015,** *1074*, 168-177.
34. Burneau, A.; Gallas, J. P., Hydroxyl Groups on Silica Surfaces. In *The Surface Properties of Silica* Legrand, A. P., Ed. John Wiley & Sons: Chichester, 1998; pp 145-312.

35. Carteret, C., Mid- and Near-Infrared Study of Hydroxyl Groups at a Silica Surface: H-Bond Effect. *J. Phys. Chem. C* **2009,** *113*, 13300-13308.
36. Jeffrey, G. A., *An Introduction to Hydrogen Bonding*. Oxford University Press: New York and Oxford, 1997.
37. Colthup, N. B.; Daly, L. H.; Wiberley, S. E., *Introduction to Infrared and Raman Spectroscopy*. Academic Press: New York, 1975; p 547.
38. Nakamoto, K., *Infrared and Raman Spectra of Inorganic and Coordination Compounds*. John Wiley & Sons: New York, 1986; p 232.
39. Tosoni, S.; Pascale, F.; Ugliengo, P.; Orlando, R.; Saunders, V. R.; Dovesi, R., Quantum Mechanical Calculation of the OH Vibrational Frequency in Crystalline Solids. *Mol. Phys.* **2005,** *103*, 2549-2558.
40. Xing, J.-Y.; Buffet, J.-C.; Rees, N. H.; Norby, P.; O'Hare, D., Hydrogen Cleavage by Solid-Phase Frustrated Lewis Pairs. *Chem. Commun.* **2016,** *52*, 10478-10481.
41. Zhang, S.; Huang, Z.-Q.; Ma, Y.; Gao, W.; Li, J.; Cao, F.; Li, L.; Chang, C.-R.; Qu, Y., Solid Frustrated-Lewis-Pair Catalysts Constructed by Regulations on Surface Defects of Porous Nanorods of CeO_2. *Nature* **2017,** *8*, 15266.
42. Huang, Z.-Q.; Liu, L.-P.; Qi, S.; Zhang, S.; Qu, Y.; Chang, C.-R., Understanding All-Solid Frustrated-Lewis-Pair Sites on CeO_2 from Theoretical Perspectives. *ACS Catal.* **2018,** *8*, 546-554.
43. Świderek, K.; Marti, S.; Tuñón, I.; Moliner, V.; Bertran, J., Peptide Bond Formation Mechanism Catalyzed by Ribosome. *J. Am. Chem. Soc.* **2015,** *137*, 12024-12034.
44. Musso, F.; Sodupe, M.; Corno, M.; Ugliengo, P., H-Bond Features of Fully Hydroxylated Surfaces of Crystalline Silica Polymorphs: A Periodic B3LYP Study. *J. Phys. Chem. C* **2009,** *113*, 17876-17884.
45. Dovesi, R.; Orlando, R.; Erba, A.; Zicovich-Wilson, C. M.; Civalleri, B.; Casassa, S.; Maschio, L.; Ferrabone, M.; De La Pierre, M.; D'Arco, P.; Noël, Y.; Causà, M.; Rérat, M.; Kirtman, B., CRYSTAL14: A Program for the Ab Initio Investigation of Crystalline Solids. *Int. J. Quantum Chem.* **2014,** *114*, 1287-1317.
46. Frisch, M. J.; Trucks, G. W.; Schlegel, H. B.; Scuseria, G. E.; Robb, M. A.; Cheeseman, J. R.; Scalmani, G.; Barone, V.; Mennucci, B.; Petersson, G. A.; Nakatsuji, H.; Caricato, M.; Li, X.; Hratchian, H. P.; Izmaylov, A. F.; Bloino, J.; Zheng, G.; Sonnenberg, J. L.; Hada, M.; Ehara, M.; Toyota, K.; Fukuda, R.; Hasegawa, J.; Ishida, M.; Nakajima, T.; Honda, Y.; Kitao, O.; Nakai, H.; Vreven, T.; J. A. Montgomery, J.; Peralta, J. E.; Ogliaro, F.; Bearpark, M.; Heyd, J. J.; Brothers, E.; Kudin, K. N.; Staroverov, V. N.; Keith, T.; Kobayashi, R.; Normand, J.; Raghavachari, K.; Rendell, A.; Burant, J. C.; Iyengar, S. S.; Tomasi, J.; Cossi, M.; Rega, N.; Millam, J. M.; Klene, M.; Knox, J. E.; Cross, J. B.; Bakken, V.; Adamo, C.; Jaramillo, J.; Gomperts, R.; Stratmann, R. E.; Yazyev, O.; Austin, A. J.; Cammi, R.; Pomelli, C.; Ochterski, J. W.; Martin, R. L.; Morokuma, K.; Zakrzewski, V. G.; Voth, G. A.; Salvador, P.; Dannenberg, J. J.; Dapprich, S.; Daniels, A. D.; Farkas, O.; Foresman, J. B.; Ortiz, J. V.; Cioslowski, J.; Fox, D. J. *Gaussian 09*, Gaussian Inc.: Wallingford CT, 2013.
47. Becke, A. D., Density-Functional Thermochemistry. III. The Role of Exact Exchange. *J. Chem. Phys.* **1993,** *98*, 5648-5652.
48. Dewar, M. J. S.; Thiel, W., Ground States of Molecules. 38. The MNDO Method. Approximations and Parameters. *J. Am. Chem. Soc.* **1977,** *99*, 4899-4907.
49. Lee, C.; Yang, W.; Parr, R. G., Development of the Colle-Salvetti Correlation-Energy Formula into a Functional of the Electron Density. *Phys. Rev. B* **1988,** *37*, 785-789.

50. Vreven, T.; Morokuma, K., On the Application of the IMOMO (Integrated Molecular Orbital + Molecular Orbital) Method. *J. Comput. Chem.* **2000,** *21*, 1419-1432.
51. Grimme, S.; Ehrlich, S.; Goerigk, L., Effect of the Damping Function in Dispersion Corrected Density Functional Theory. *J. Comp. Chem.* **2011,** *32*, 1456-1465.
52. McQuarrie, D., *Statistical Mechanics*. Harper and Row: New York, 1986.

TOC